Technical Proposal
ONRBAA13-003 for program 331

Fluid structure interaction for marine energy and coastal ecology

Brown University, Providence, RI 02912

Technical contact
Shreyas Mandre
Assistant Professor, School of Engineering
Box D, Brown University,
Providence RI 02912
Phone: (401) 863-2602 Fax: (401) 863-9028
Shreyas_Mandre@brown.edu

Administrative contact
Ms. Eva Faling, Esq.
Assistant Director-Pre Award Services
Office of Sponsored Projects
Box 1929, Brown University,
Providence, RI 02912
Phone: (401) 863-3630 Fax: (401) 863-7292
Eva_Faling@brown.edu

Proposed period of performance
May 15, 2013 – May 14, 2016

Project title: Fluid structure interaction for marine energy and coastal ecology
Principal investigator: Shreyas Mandre
Institution: Brown University
Total funds requested: $560,000

Abstract: The goal of this project is to enable and facilitate an informed trade-off between tidal power conversion and coastal ecological preservation. The US is estimated to have about 50 GW of tidal current power, and harnessing it will contribute to the Department of Navy's goal of generating 50% of its onshore power from alternative sources. Extracting this resource is speculated to have a variety of environmental and ecological impact. We propose a systematic analysis of the fundamentals behind the energy-ecology trade-off.

Tidal current powers the transport system of a healthy marine ecosystem by carrying seeds, spores, eggs, larvae, nutrients, and sediment over large distances. The currents passing through vegetation also induce turbulence, which mixes the fluid locally, thus bringing fresh supply of nutrients to the surface of the organisms and carrying away waste products. There is overwhelming evidence that the role of tides in maintaining the ecosystem is critical. One of the most important processes operating in marine grass canopies is fluid-vegetation interaction, where grass blades wave synchronously, much like wind induced waves on terrestrial grass. We develop a mathematical model for marine grass canopies, approximating the grass field as a continuum and unleash a host of analytical and numerical methods to seek the fundamental principles underlying the transport processes assisted by fluid vegetation interaction.

Any device extracting power from tidal currents must slow the flow down and introduce turbulence in its wake. The nature of turbulence introduced depends on the device, and we argue that an oscillating hydrofoil technology, which we are independently developing, is capable of perturbing the flow in an infinite number of ways whilst extracting the same amount of power from it. We develop a systematic optimal control framework to describe the power conversion abilities of the oscillating hydrofoil, to extract maximum energy from the flow, while obeying the constraints set by the ecological processes.

The anticipated outcome of the research is the development of a framework to treat the inevitable trade-off that not only effects tidal power but possibly also other renewable power sources. In collaboration with other researchers and entrepreneurs at Brown and world-wide, we are designing a pilot scale system of an oscillating hydrofoil power conversion system expected to be deployed in 2015. Such a deployment will provide an excellent opportunity not only to study power conversion characteristics of the device but also interaction of the physical device with the environment and the simulated outcome of any environmental policy. This research forms an integral component for spanning the interdisciplinary range from engineering to marine ecology to environmental policy.

Contents

1 Introduction to tidal in stream technology

Current technologies to capture tidal, river and ocean current typically use horizontal or vertical axis turbines – close relatives of the wind turbines – for converting the kinetic energy of the fluid to electricity and are optimized for a narrow range of operating conditions. The turbine installed by Verdant Power in the East River, New York, NY is shown in figure 1 as an example. The market movement towards in stream devices and away from tidal barges is mostly in response to the environmental impact of large civil structures in the coastal areas.

1.1 Technology Tidal turbines perform poorly from an economic perspective in harnessing this power because they apply principles from wind energy conversion to a resource with a superficially similar but fundamentally different nature. The principle difference is that wind is plentiful at higher altitudes, while tidal currents are stronger in shallow water depths. As economy of scale forces the design towards a larger turbine size, a shallow water depth limits the installation of a tidal turbine any larger, and this eliminates many prime sites. Moreover, as we discuss later, we have no control over the flow disturbance an individual turbine or a turbine farm generates in its wake without changing the power output. Of the infinite ways the flow can be perturbed whilst extracting energy, the turbines choose one fixed way to perturb the flow.

This limitation is partially overcome by vertical axis turbines and oscillating hydrofoils such as the devices manufactured by PulseTidal[5], but oscillating hydrofoils offer the most advantage in terms of hydrodynamic characteristics and flexibility. The principle of operation of the oscillating hydrofoils, schematically shown in figure 2, is similar to that of turbines with linear rather than rotational blade motion. The orientation of the hydrofoil relative to the flow, called the hydrofoil pitch, is dynamically adjusted such that oncoming flow pushes the hydrofoil downwards on a down stroke and upwards on a up stroke[46, 45]. The energy provided to alter the hydrofoil pitch is more that compensated for by the work done by the flow on the heaving mode of the hydrofoil. Other mechanisms, such as cables and cylinders can be driven to oscillation using vortex shedding and have been proposed for wind power conversion[39]. However, these geometries are not as efficient as a streamlined hydrofoil in generating and controlling hydrodynamic force.

Oscillating hydrofoils have many advantages over turbines in terms of site adaptability and large-scale deployment. Although turbine blades also employ a streamlined geometry, the blade rotation means that the efficiency varies from the root to tip due to the varying blade velocity, In contrast, all locations on an oscillating hydrofoil move at the same speed and hence achieve uniform efficiency. It is estimated by PulseTidal that for this reason, and the fact that the square area traversed by their hydrofoil is larger by a factor of $4/\pi$ than the circular area traversed by the turbine blades, their device extracts 4 times as much energy as turbine spanning the same size (see www.pulsetidal.com). Uniform hydrofoils offer ease of manufacturing, which the turbine blades do not. Replacing the hydrofoil with one of smaller size adapts the system for sites with faster currents, whereas the turbine blades can not be exchanged so conveniently or cheaply. Tip losses in rotary turbines significantly reduce their performance, while a hydrofoil can be trivially expanded by installing another

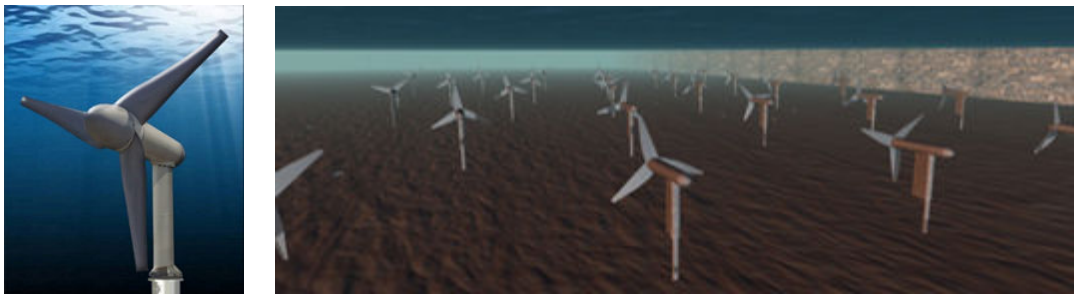

(a) (b)

Figure 1: (a) An example of a tidal turbine and (b) an artist's rendition of a tidal farm designed by Verdant Power. An array of six of these turbines was tested and demonstrated in the East River, New York NY, and a 1 MW commercial pilot farm is planned. Up to 30 turbines will be incrementally added to the farm. (source and image credit verdantpower.com)

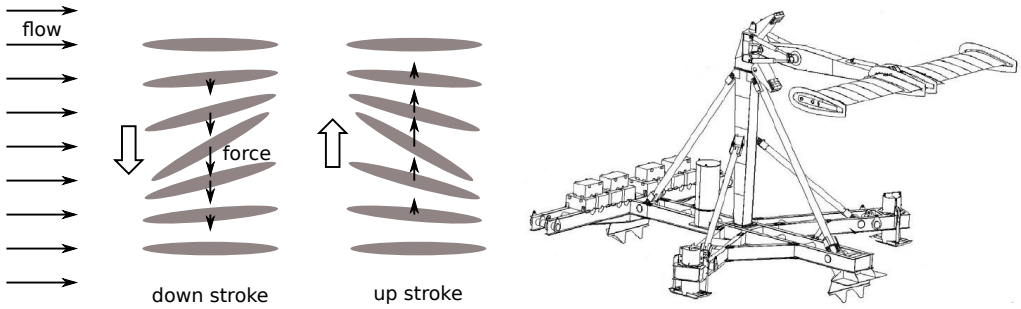

(a) (b)

Figure 2: (a) Principle of operation behind power conversion by oscillating hydrofoil systems and (b) a isometric view of the Stingray oscillating hydrofoil device assembly. The hydrofoil is tilted downwards on a down stroke (left) and upwards on an up stroke (right). As a result, the hydrodynamic force on the hydro foil always points in the direction of the motion, and the flow does mechanical work on the hydrofoil, which is used to drive a generator.

hydrofoil adjoining it, and the tip effects can be consolidated or even captured akin to the mechanism achieved in the V-shaped flight formations of migratory birds. Turbines prohibit close placement due to hydrodynamic interference. Conversely, a long hydrofoil can be broken up into smaller hydrofoils sections to suit other design constraints without any loss in hydrodynamic efficiency. Lastly, while the turbine geometry permanently blocks the waterway, a hydrofoil can be stopped and stowed near the bed so as to give way to passing ships.

The most important advantage of the oscillating hydrofoil is that for fixed energy extraction rate, it provides a possible mechanism to perturb the flow in an infinite number of ways. The flexibility arises from the choice of pitching and heaving trajectory of the hydrofoil. The pitch and heave trajectory of the hydrofoil can be chosen from an infinite-dimensional space of all periodic function, and thus a set of trajectories *could* lead to the conversion of identical

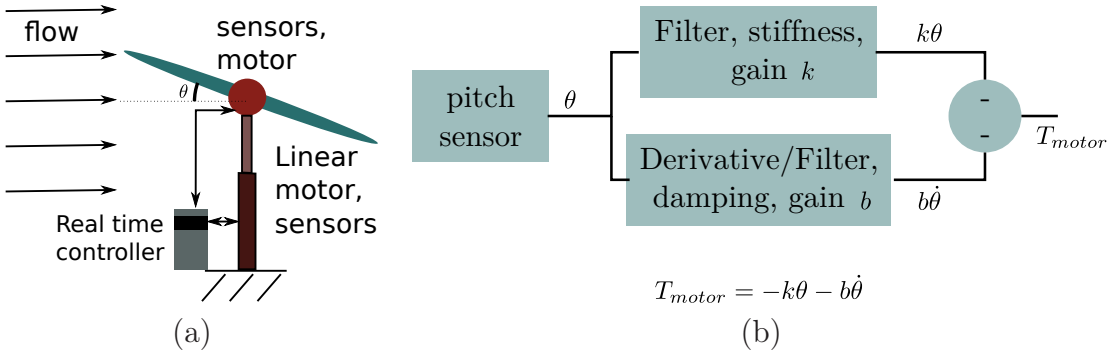

Figure 3: (a) A schematic setup of the cyber-physical oscillating hydrofoil system, and (b) the control feedback loop for the pitch degree of freedom. A similar control loop is implemented for the heave degree of freedom simulating a torsional spring and damper.

average power but different flow perturbations. The true merit of the method is unleashed when we allow unsteady fluid dynamic effects such as leading edge vortex shedding, vortex recapture, transient boundary layer separation, etc to play a role. These effects are believed to be underlying the superior aerodynamic performance of birds and insects in comparison to performance dictated by quasi-steady aerodynamics, and we expect a systematic exploitation of the unsteady effects to render the oscillating hydrofoil with better power extraction capabilities in comparison to devices that use quasi-steady dynamics [21, 23, 40, 42, 43]. Such a flexibility needs a systematic framework to beneficially manipulate and control the infinite degrees of freedom. A fundamental fluid dynamic analysis of the extent of possibilities for such an hydrofoil is the objective of this project.

A group of fluid dynamicists, ecologists and entrepreneurs at Brown led by the PI are selected for and currently negotiating an award from the Department of Energy (DOE) to build a proof of concept and commercialize this technology for tidal power conversion, along with another from the Air Force Office of Scientific Research (AFOSR) to examine the fundamental fluid dynamics for wind power conversion. We control the trajectory of the hydrofoil using a set of sensors and actuators for the pitching and heaving degrees of freedom and an onboard real-time controller – the so-called *cyber-physical system* (see figure 3, where the feedback loop simulates a torsional spring). The actuator also performs as a generator when work is done by the flow on the hydrofoil, and in this way tidal kinetic energy is converted to electricity. The control loop can be used to execute any arbitrary stroke of the hydrofoil. We have the experimental system in a wind-tunnel for the AFOSR project and the corresponding system in the water channel is expected to be funded by the DOE award. In the commercial version of the device, force and torque sensors are used to experimentally measure the energy extracted from the flow and the focus is to develop real-time optimization algorithms to maximize the average power extracted as a function of the imposed hydrofoil trajectory. The goal of the DOE high-risk-high-reward commercialization project is to design a pilot system by the end of 2013. In the first phase, the objective is to demonstrate the feasibility of the hydrodynamics, and in the second phase to develop the power electronics for

conversion to electricity in collaboration with electrical engineers. This commercialization opportunity imparts a technological significance to the abstract hydrodynamics questions posed in this proposal and has direct impact on the proposed technology.

To our knowledge there are only two examples (both in the UK) of using oscillating hydrofoils for tidal in stream power conversion. A 150 kW prototype called Stingray was being developed by the Engineering Business Limited, but was discontinued in 2006. The second device is the Pulse device by the Pulse Tidal capable of 100 kW and they are planning a 1.2 MW device scheduled for commercial demonstration in 2014. In both systems, the hydrofoil pitch is actively controlled using a propriety protocol with special attention to maintain quasi-steady hydrodynamics over the hydrofoil. In fact, most aero- and hydrodynamic technologies that exist today (aircraft wings and blades, propellers, turbines, sails) are designed to operate under steady or quasi-steady conditions, and extreme care is taken to avoid any unsteadiness in their operation owing to our inability to develop reliable fluid dynamic control.

We propose a systematic way of theoretically analyzing the optimal control problem of the trajectory of a oscillating hydrofoil. Shape optimization (in this case of a trajectory) requires finding the solution of the fluid flow in response to the trajectory, and the gradient of the objective function (the extracted power) with respect to the trajectory. The main difficulty in developing a theoretical understanding is the computational complexity of fluid dynamics solvers at high Reynolds numbers. As the Reynolds number grows, both the Kolmogorov scale for energy dissipation as well as the time scale of the dissipation decreases, thus requiring higher spatial resolution and smaller time steps. Practically, on a stock parallel computer the direct numerical simulation of the two-dimensional flow past an oscillating hydrofoil at a Reynolds number of $O(10^4)$ takes from a few hours to a day depending upon the period of oscillations, the numerical method used, the number of processors and the speed of the computer. The calculation of the gradient (e.g. using an adjoint based method) is expected to take about the same amount of time, and an expected 10-20 iterations of the optimization algorithm implies a total run-time of weeks to months for one set of parameters. This estimate rules out parameter sweeps and increasing the Reynolds number towards more realistic values for hydrofoils and wings only worsens the situation. For this reason, approximate methods are used to accelerate the flow computation.

In §2, we describe a hybrid of boundary layer approximation and vortex methods to tackle the computational complexity. The strategy is to solve reduced equations in the boundary layer, and couple them with a vortex method outside the boundary layer. The solution in the boundary layer essentially replaces the Kutta condition imposed at the sharp edges of the hydrofoil to determine the strength and location of shed vorticity with an approximation of the governing Navier-Stokes equations. This alternative to the Kutta condition naturally applies for unsteady and high angle of attack situations, thereby providing a systematic way to address unsteady effects such as dynamic stall, leading edge separation and vortex, etc. Based on this simplified model, we propose an optimal control framework for the motion of the hydrofoil with the objective of power extraction. Similar framework can be used for related problems, such as maximizing thrust for fixed energy expenditure on a flapping

hydrofoil. We expect this part to require two years worth of work by one graduate student.

1.2 Ecology There is persuasive evidence that regions with high tidal current and wave density support ecosystems with larger biomass due to the enhanced transport and mixing of material brought about by the fluid flow. In general, a myriad of mechanisms linking hydrokinetic energy and marine bio-proliferation are suggested, and many of them lead to a positive correlation between the two variables. While our understanding of tides is still evolving[9], it is now widely accepted that lunar attraction imparts approximately 4 TW power to the oceans, out of which approximately 3/4 is dissipated near the ocean coasts (the remaining 1/4 is dissipated in internal tides [13]). There is statistical correlation between this enormous source of energy, and the biodiversity and biomass near the coastal regions of water bodies[35]. The main comparison leading to this conclusion is that of the large lakes, which provide all the necessary ingredients for life but do not support substantial tides or waves, with coastal region of the oceans, which are large enough to support tides.

The primary requirements for most common marine life are sunlight, dissolved gases, and nutrients. Sunlight penetrates only near the surface of the ocean, while the nutrients are predominantly accumulated near the ocean bed, as dead marine organisms sink to the bottom. As a result, coastal regions with shallow depths and regions of upwelling are ideal for marine life because they combine the requirement for both the resources by either having the ocean bed close to the ocean surface or transporting the nutrients from the bed to the surface. An important factor underlying the enhanced bio-proliferation in the coastal oceans is that the tides and waves constantly stir the region suspending the nutrients in the water, a mechanism not so effective in the lakes. Despite the shallow average depths of the lakes (e.g. average depth of Lake Erie is 18.6 m and that of Lake Chad is 4 m) and the energy input by the wind, it is the mixing caused by the tides that has the most effect on marine ecology [35]. Moreover, the enhanced transport in the momentum boundary layer formed due to flow past leaves[11, 36, 44, 41] also helps biological productivity. The corals also rely on the flow of water for transport from their tissues to the environment[17, 12]. In fact, coral reefs often develop in extreme nutrient poverty, and are overtaken by macroalgal communities in a process known as eutrophication when nutrients become abundant[7, 6, 29] and this process is also influenced by tides[22]. Thus, not only is flow induced transport and mixing an crucial ingredient in supporting marine ecology, but also the nature of the ecosystem is determined by the intensity of the mixing process. Thus, to preserve biodiversity, it is imperative to not alter the tidal mixing as much as possible. A positive aspect of such a dependence of ecology on tidal flow is that installation of tidal in stream devices can coexist with marine ecology, and become an integral part as both the ecology and technology learns and adapts to each other's presence. If these devices allow flexibility in their operation, they may even be used to control both the composition and quantity of biomass.

The mechanism underlying the transport characteristics vary according to the length scale under consideration, and simple estimates of the mixing time scale help us understand the relevance of tidal flow and fluid-vegetation interaction. Molecular diffusion transports nutrients from the immediate surface of the organism through the diffusion boundary layer. Once outside this boundary layer, advection due to the flow is the main mechanism for trans-

port of species. Turbulence and mixing induced by flow around sufficiently sparse[33] marine flora dominates the mixing process, but the flow itself does not penetrate the vegetation if it is sufficiently dense[34]. Mixing is quantified in terms of a turbulent diffusivity, which scales as $\kappa = Ud$ with characteristic flow speed U around the vegetation and a characteristic length d, such as the spacing between neighboring stems or leaves[33]. The fast tidal flow (~ 1 m/s) penetrates only near the surface of the dense vegetation canopy, whereas in the interior of the vegetation, the flow is substantially decelerated (~ 1 cm/s)[34]. A characteristic length scale in the range 1–10 cm yields a diffusivity of $D \approx 10^{-3} - 10^{-4}$ m^2/s. For a vegetation canopy of size L =1-10 m, the diffusion time scale for mixing turns out to be $L^2/D \approx 10^6 - 10^3$ s, or between a week and a day. To contrast that in the absence of the tides, molecular diffusion would have taken at least decades to bring about such mixing.

The flexibility of the vegetation enhances this mixing dramatically. The oscillatory motion of the vegetation increases the scale of the flow speed in the canopy, while long scale synchronization of these oscillations increases the length scale. Such a waving motion of vegetation is observed in eel grass canopies[1], and enhances the fluid velocity to O(10 cm/s) on the scale of the wavelength of about 1 m, thus increasing the turbulent diffusivity to O(0.1 m^2/s). This increase in the turbulent diffusivity implies that the mixing time scale is a few seconds, comparable to the advection time scale L/U of flow above the canopy, and gives a chance for biological material carried by the flow to penetrate the canopy. It is observed that in this manner, mussel larvae penetrate the eel grass canopy, and settle near regions of slow flow, thereby directly affecting their life cycle[15]. Such a "fluid-vegetation" interaction clearly plays a significant role in determining the spawning site for mussels[15], and also for seeds, spores and other biological matter[19], and possibly also for sediment. Understanding fluid-vegetation interaction is central to a successful description of the transport through vegetation.

In §3, we describe a systematic experimental and theoretical framework for determining the characteristics of such spontaneous fluid-vegetation oscillations. The theoretical framework consists of representing the grass as a distributed body force equal to the hydrodynamic force per unit length on the grass blade times the area number density of grass blades. This hydrodynamic force is parametrized as a fluid drag motivated by experimental measurements[33, 34]. The two-dimensional version of this model is subjected to a host of numerical and analytical methods for characterizing the resulting flow and vegetation deformation and the mixing characteristics. This analysis is supplemented by simple experiments in a soap film tunnel. Flexible filaments introduced in the flow of soap film between two wires emulates in two dimensions the flow past a vegetation canopy. the PI's lab has developed the capability to measure velocity field using high speed particle image velocimetry using frame rates of up to 1000 frames/sec, to provide detailed comparison and guidance for mathematical modeling. We expect this part to require two years worth of effort by one graduate student.

1.3 Trade-off between power extraction and ecological preservation Once the optimal control and the ecological mixing rates are characterized, the trade-off between power extraction and ecological preservation in optimal control formulation takes the form

of a constrained optimization. In this proposal we focus on the trade-off on the local scale as a first step in preparation for studying the trade-off on the scale of an estuary network to future. The mixing in the absence of power extraction is considered to be known and will be treated as an ecological parameter for local plant canopies, characterized from the previous part of the project. When power is extracted from the flow, the rate of mixing is reduced due to the slower flow speeds. This reduction in mixing rate is expected to be compensated by the vortices induced by the oscillating hydrofoil trajectory. Such a compensation relies on our mechanism to extract marginally reduced amounts of energy but capable of inducing varying amounts of vorticity in the wake, which the tidal turbines do not have.

The main theoretical question is whether this framework is reasonable, at least in the mathematical sense. Admittedly, there are a plethora of parameters and effects eliminated from consideration in favor of the framework's simplicity. In the absence of such complicating factors, can we demonstrate theoretically that such a trade-off is cleanly achieved? This is the main premise on which we hypothesize a superior performance from an ecological perspective from the oscillating hydrofoil we are developing to commercialize. A necessary condition for the success is the theoretical demonstration of this trade-off as stated in the previous paragraph, and as rationalized in the next.

It is reasonable that in the absence of any tidal current, the hydrofoil may be actuated to introduce a certain amount of mixing at the expense of energy (what a fan does in a domestic living room). Thus it appears reasonable to suppose, and the objective of this project to rigorously demonstrate, that in the presence of the tidal current, a part of the kinetic energy of the flow can be extracted, while another part is used to compensate for the reduced mixing. Crude but conceptually equivalent is having a tidal turbine for energy extraction and a propeller for inducing extra mixing, and the question is how much more power does the turbine extracts than the fan expends. We connect the optimization framework for the oscillatory hydrofoil and the fluid-vegetation interaction in §4. We expect a one year collaborative effort between the two graduate students who performed the research proposed in the previous two subsections.

2 Optimal control of oscillating hydrofoil

Consider the two-dimensional flow in the xy-plane of a fluid in a channel of finite depth H past an elliptical hydrofoil of semi-major axis non-dimensionalized to unity and semi-minor axis ϵ (see figure 4). The hydrofoil moves with two degrees of freedom, heave $h(t)$ and pitch $\alpha(t)$, where both are periodic functions of time t. Once the transients have dissipated, the periodic force and torque on the hydrofoil are denoted $F(t)$ and $M(t)$, and the average rate of work done by the flow on the hydrofoil is

$$P[h,\alpha] = \frac{1}{T}\int_0^T \left[F(t)h(t) + M(t)\alpha(t)\right]\ dt. \tag{1}$$

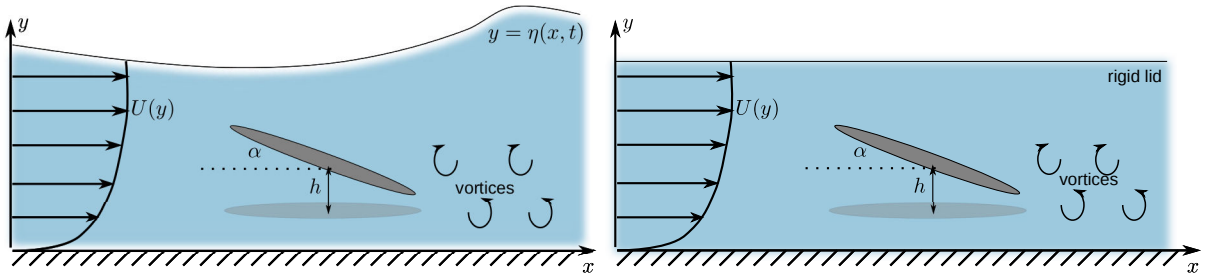

Figure 4: Schematic setup for the mathematical model for optimal control of oscillating hydrofoil. Two cases are considered – a free interface (left) and a rigid lid (right).

The force and torque themselves are given in terms of the fluid stress tensor $\boldsymbol{\Sigma}$ and pressure p as

$$F = \int_A (-p\boldsymbol{\mathcal{I}} + \boldsymbol{\Sigma}) \cdot \boldsymbol{n} dA, \quad M = \boldsymbol{z} \cdot \int_A \boldsymbol{r} \times (-p\boldsymbol{\mathcal{I}} + \boldsymbol{\Sigma}) \cdot \boldsymbol{n} dA, \tag{2}$$

where $\boldsymbol{\mathcal{I}}$ is the identity tensor, A the surface of the hydrofoil, $\boldsymbol{n}$ is the unit normal to the surface, $\boldsymbol{r}$ the position vector on the surface and $\boldsymbol{z}$ the normal in the z direction (perpendicular to the plane of the paper). The stress tensor is given by the Newtonian constitutive law, and the velocity fields $\boldsymbol{u}$ satisfies the Navier-Stokes equations as

$$\boldsymbol{\Sigma} = \frac{1}{\mathrm{Re}}(\boldsymbol{\nabla u} + \boldsymbol{\nabla u}^T), \quad \boldsymbol{u}_{,t} + \boldsymbol{u} \cdot \boldsymbol{\nabla u} + \boldsymbol{\nabla} p = \frac{1}{\mathrm{Re}} \nabla^2 \boldsymbol{u}, \quad \boldsymbol{\nabla} \cdot \boldsymbol{u} = 0. \tag{3}$$

where Re is the Reynolds number. These equations are supplemented with the boundary conditions of no slip at the bottom $\boldsymbol{u} = 0$, no traction $\boldsymbol{\Sigma} \cdot \boldsymbol{n}$ at the free interface $y = \eta(t)$ obeying a kinematic condition $\eta_t + u\eta_x = v$, and ideally infinite extent in the x direction with the velocity approaching a prescribed function $u = U(y)$ upstream. We also allow the simpler possibility of considering the somewhat artificial but computationally convenient condition (called the "rigid lid" condition) of no shear stress and no normal velocity on a fixed top boundary. The goal is to solve the optimization problem

$$\max_{h,\alpha} P[h, \alpha] \text{ subject to (2) and (3).} \tag{4}$$

The Reynolds number of tidal flow is typically large and therefore the flow is turbulent. The upstream profile is blunt and may be approximated with $U(y) = U$=constant. The flow around but away from the hydrofoil may be approximated by a non-circulatory part $\boldsymbol{u}_{nc} = \boldsymbol{\nabla}\phi$ due to a potential ϕ and a circulatory part due to vorticity shed in the wake of the hydrofoil. Finite amplitude gravity waves and motion of the hydrofoil can be incorporated in this framework using boundary integral methods [24, 37] for the non-circultory potential using a Greens function formulation,

$$\mathrm{pv} \int_B G(\boldsymbol{x}, \boldsymbol{r}) \boldsymbol{\nabla}\phi(\boldsymbol{r}) \cdot \boldsymbol{n} - \phi(\boldsymbol{r}) \boldsymbol{\nabla} G(\boldsymbol{x}, \boldsymbol{r}) \cdot \boldsymbol{n} \; d\boldsymbol{r} = \frac{1}{2}\phi(\boldsymbol{x}), \tag{5}$$

where $G(\boldsymbol{x},\boldsymbol{r}) = -\log|\boldsymbol{x}-\boldsymbol{r}|/2\pi$ is the fundamental solution of Laplace equation, pv denotes principle value of the integral, and B is the boundary of the computational domain. On the no-normal-flow boundary, $\boldsymbol{\nabla}\phi\cdot\boldsymbol{n}$ is known but ϕ is unknown, while on the free surface where the pressure is known, the Bernoulli equation

$$\phi_{,t} + \frac{1}{2}|\boldsymbol{\nabla}\phi|^2 + p + gy = \text{ constant} \tag{6}$$

gives an evolution equation for ϕ, which can be integrated in time for ϕ, but $\boldsymbol{\nabla}\phi\cdot\boldsymbol{n}$ is unknown. The discretization of (5) provides equations for the unknown ϕ and $\boldsymbol{\nabla}\phi\cdot\boldsymbol{n}$ at every grid point on the boundary. The value of ϕ and $\boldsymbol{\nabla}\phi\cdot\boldsymbol{n}$ from the solution can be used to advect the boundary, both the elliptical hydrofoil and the free surface. The PI has experience with using these methods and adapting them for different problems during his research on droplet impact and splashing[27, 25, 28].

To determine the circulatory part of the flow, one way to proceed efficiently is to take the $\mathrm{Re}\to\infty$ and $\epsilon\to 0$ (thin plate) limit, shed point vortices from the edges of the plate and impose the Kutta condition to determine the strength of the vortices. The vortices provide the circulatory part of the flow and are themselves advected with the desingularized part of the flow

$$\boldsymbol{u}_c(\boldsymbol{x},t) = \sum_{j=1}^{N} \frac{(\boldsymbol{x}-\boldsymbol{x}_j)\times\boldsymbol{z}}{2\pi|\boldsymbol{x}-\boldsymbol{x}_j|^2}\,\Gamma_j, \quad \frac{d\boldsymbol{x}_k}{dt} = \boldsymbol{u}_{nc}(\boldsymbol{x}_k) + \sum_{j=1,j\neq k}^{N} \frac{(\boldsymbol{x}_k-\boldsymbol{x}_j)\times\boldsymbol{z}}{2\pi|\boldsymbol{x}_k-\boldsymbol{x}_j|^2}\,\Gamma_j. \tag{7}$$

where the j^{th} vortex of strength Γ_j is at $\boldsymbol{x}_j(t)$. This approach has been used to study the falling of cards, heaving plates and flutter[18, 32, 30, 31, 38, 2]. There is however, one major drawback of these methods; at low angles of attack the flow may advect one of the shed vortex parallel to the hydrofoil boundary and thus cause a singular behavior because of the image vortex across the boundary[18, 30]. Jones and Shelley[18] stated that "this restricts our investigation to high effective angles of incidence", while Michelin and Lewellyn-Smith[30] called it the "main limitation of the present method", whereas Alben[2] decided *ad hoc* that a vortex is not shed. Moreover, the Kutta condition does not apply for smooth bodies, since there are no velocity singularities in flow around them. No simple method exists for determining the vortex shedding from smooth bodies (see however the vortex method for boundary layers[10], which is not simple).

We provide a conceptually simple and physically accurate method for determining the location and strength of vortex shedding. This methods separates the domain in two regions, the outer region where the vortex methods are applied, and an inner region near the elliptical hydrofoil where the flow satisfies the boundary layer approximation of the Navier-Stokes equations. For simplicity, we write the boundary layer equations in elliptical coordinates $x = \cosh\xi\cos\theta/\cosh\xi_0$, $y = \sinh\xi\sin\theta/\cosh\xi_0$ moving with the hydrofoil, where θ is the tangential coordinate and $0 < \xi - \xi_0 < \xi_{\max} - \xi_0 = O(\mathrm{Re}^{-1/2})$ is the normal boundary layer coordinate (ξ_0 is chosen so that the aspect ratio is $\tanh\xi_0 = \epsilon$). The tangential $u_\theta = O(1)$

and normal components $u_\xi = O(\mathrm{Re}^{-1/2})$ of velocity satisfy,

$$g u_{\theta,t} + \left(g u_\theta^2\right)_{,\theta} + (g u_\theta u_\xi)_{,\xi} + p_{,\theta} = \frac{1}{\mathrm{Re}} u_{\theta,\xi\xi} + \text{ fictitious forces}, \tag{8}$$

$$(g u_\theta)_{,\theta} + (g u_\xi)_{,\xi} = 0, \qquad p_{,\xi} = 0, \tag{9}$$

where subscript followed by a comma denote partial differentiation, $g(\theta) = (\sinh^2 \xi_0 + \sin^2 \theta)/\cosh^2 \xi_0$ is the local metric in the boundary layer, and the fictitious forces arise from the rotation and acceleration of the reference frame attached to the moving hydrofoil. The pressure in the boundary layer approximation is determined by using a Bernoulli equation for the outer flow, and that eliminates the need to solve a Poisson problem for the pressure and reduces the computational time significantly.

The boundary layer equation accurately models the generation of vorticity near the boundary, but the crucial piece of this method is the mechanism for shedding vorticity into the outer region. Hence the core of this proposal is identifying alternatives to the Kutta condition based on the instantaneous solution in the boundary layer. Vorticity can not diffuse out of the boundary layer because viscous effects are negligible outside the boundary layer. Thus vorticity must be advected out of the boundary layer at or near the instantaneous outflow stagnation points in the boundary layer.

We are not the first to identify this process of vorticity generation; it is in fact commonly known and described in textbooks[4, 20]. As much as this process is conceptually accepted, we have found no translation of the conceptual model into a mathematical framework to facilitate computation of vortex shedding. The objective of such a mathematical model is to replace the Kutta condition based on the singularity in the outer flow with another condition based on the properties of the boundary layer solution. We highlight that a spectrum of methods with varying accuracy and computational cost are possible.

The spectrum of methods may be understood by considering that at the outflow stagnation points, a continuous distribution of vorticity leaves the boundary layer into the outer region. The degree of detail in the discrete vortex representation of this vorticity distribution and the accuracy to which the discretization captures the salient features of the vorticity field determines the computational speed and accuracy of the method. The boundary layer equation are symmetric under the reflection transformation $\xi \to -\xi$ and $u_\xi \to -u_\xi$. As a result, vorticity can enter or leave the boundary layer from either the solid wall $\xi = \xi_0$ or by symmetry the outer region $\xi = \xi_{\max}$. As long as the inner limit of the outer solution agrees with the outer limit of the inner solution given by

$$g u_{\theta,t} + \left(g u_\theta^2\right)_{,\theta} + (g u_\theta u_\xi)_{,\xi} + p_{,\theta} = \text{ fictitious forces}, \quad (g u_\theta)_{,\theta} + (g u_\xi)_{,\xi} = 0, \tag{10}$$

no exchange of vorticity occurs between the two regions. As the vorticity is transported towards $\xi = \xi_{\max}$ at the outflow stagnation point, the outer limit of the inner solution starts to differ from the inner limit of the outer solution and a discrepancy between inner limit of the outer flow and the outer limit of the inner flow develops. In a step equivalent to asymptotic matching of the boundary layer to the outer flow, this discrepancy can be

resolved by introducing suitable vorticity in the region just outside the $\xi = \xi_{\max}$, and this is our proposed method for shedding vorticity. The shed vorticity may take the form of a single point vortex, or depending on the scheme many closely spaced point vortices so as to better approximate the shed vorticity distribution and further reduce the discrepancy. The computational speed depends on the number of point vortices in the flow at any time, and therefore introducing more vortices slows down the computation, but at the same time increases the fidelity of the asymptotic matching. The particular compromise we choose is to shed two point vortices from every outflow stagnation point best fit to minimize the discrepancy. Such a scheme adequately addresses the need for a wider class of situation than the Kutta condition does; for example, a static hydrofoil aligned with the flow sheds a dipolar distribution of vorticity forming the wake behind it, a fact not captured by the Kutta condition, but naturally falling within the possibility of our choice. Admittedly, the boundary layer equations are are asymptotically invalid near the outflow stagnation point, but we expect our method similar in spirit to the Kutta condition – a hueristic condition that represents physics accurately in an appropriate parameter range.

The numerical solution is used in the core of optimization process for objective function evaluation. The trajectory of the hydrofoil is parametrized in terms of the frequency ω, the amplitude and the phase of the Fourier modes

$$h(t) = \sum_{j=1}^{n} h_j \sin(\omega t + \psi_j), \qquad \alpha(t) = \sum_{j=1}^{n} \alpha_j \sin(\omega t + \chi_j), \tag{11}$$

and this computational method is used to solve for the mean power extracted. The power extracted is then maximized as a function of h_j, α_j, ψ_j and χ_j using a simple gradient descent method or a quasi-Newton BFGS method for $n = 1$ and the optimal is used as the initial guess for gradient descent with $n = 2, 3, 4, \ldots$. This process is stopped when increasing n yields marginal returns. The outcome of this optimization is an unconstrained optimal stroke and an optimum power conversion $P_{\max}$, which may be converted to a hydrodynamic efficiency of the hydrofoil using $C_P = P_{\max}/\frac{1}{2}\rho U^3 A$, and compared with the efficiency of turbines. But more importantly, the properties of the optimum provide us with a concrete basis to compare with our experimental effort, which are being performed independently in collaboration with Kenneth Breuer, a mechanical engineer at Brown.

3 Mixing induced by tidal flow

Consider a uniform marine grass (or other vegetation) canopy of height h in a channel of depth H (figure 5, we ignore the presence of a hydrofoil in this part). We model the influence of the grass in the mean field as a continuum body force found by averaging over an ensemble of grass blades in a continuum control volume. The fluid flow velocity $\boldsymbol{u}$ satisfies the dimensional Navier-Stokes equations

$$\rho\left(\boldsymbol{u}_t + \boldsymbol{u}.\boldsymbol{\nabla}\boldsymbol{u}\right) = -\boldsymbol{\nabla}p + \mu\boldsymbol{\nabla}^2\boldsymbol{u} + \mathbf{f} + \rho\mathbf{g} \tag{12}$$

where μ is an effective turbulent viscosity, $\mathbf{g}$ is gravity, ρ is density of fluid, and $\mathbf{f}$ is body force per-unit volume exerted by the grass on the fluid. Boundary conditions include no-slip at the

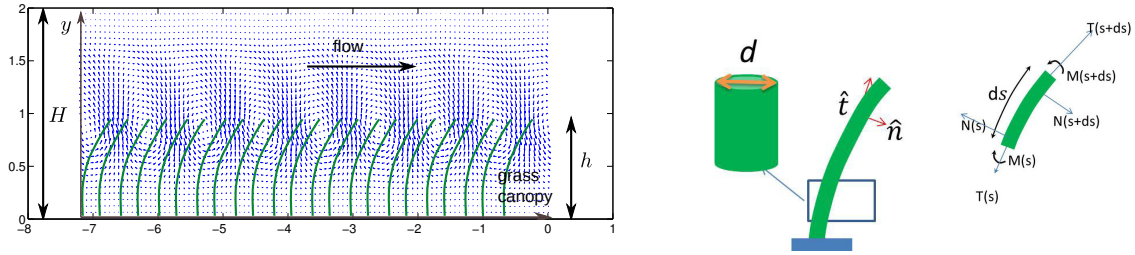

Figure 5: Schematic setup for the flow domain with arrows showing a computed growing eigenode (left) and the mechanics of an individual grass blade deformation (right).

bottom bed and rigid lid at the top (or no-slip at the top to correspond to the experiment we perform). Estimates for the turbulent diffusivity and its dependence on various geometric and flow parameters are available[33], but for simplicity we hold it to be a constant at a representative value. In the continuum limit, the grass blade orientation is assumed to be a field, and the body force is approximated to be in a mean field approximation as

$$\mathbf{f} = -N\mathbf{f_d}, \quad \mathbf{f_d} = C_N \rho \boldsymbol{u}_N^2 d\hat{n} + C_T \rho \boldsymbol{u}_T^2 d\hat{t} \tag{13}$$

where $\boldsymbol{u}_T$, $\boldsymbol{u}_N$ are velocity vector along and normal to grass, N is the area density of grass blades and the parametrization of drag is inspired by experimental measurements[33, 34]. The orientation of grass can be obtained by solving force and torque balance equation together with a constitutive relation relating bending moment M to curvature κ,

$$\frac{\partial}{\partial s}\left(T\hat{t} + N\hat{n}\right) + \mathbf{f_d} + \mathbf{f_{buoy}} = 0, \quad \frac{\partial M}{\partial s} - N = 0, \quad M = B\kappa, \tag{14}$$

where s is the arc-length along the grass blade, $\mathbf{f_{buoy}}$ is the force of buoyancy on the submerged grass blade as defined in figure 5.

Analysis of this model includes (i) numerical solution of the model in the presence of grass using a finite different PDE integrator developed in-house and by our collaborator Amala Mahadevan, WHOI, (ii) a linear stability analysis to isolate and understand the threshold for waving, (iii) a weakly nonlinear analysis to understand the saturation of the wave amplitude, and (iv) the response of the canopy to vortices in the flow, like those generated by the oscillating hydrofoil. The PI has extensive experience with these techniques from his previous research[3, 26].

We present some preliminary results on the linear stability of rigid grass to provide the reviewer with a flavor of the proposed research. The prominent model for explaining the synchronous waving is an instability of the shear flow that develops because of the drag from the grass, even if it is rigid[14]. Since rigid grass blades also impose the drag on the fluid, it was proposed and experimentally verified that the flow becomes unstable to vortices, and had the grass being flexible, it would have waved in response to these vortices. Inspired by the observations that the vortex frequency is $\Delta U/\delta_s$, where ΔU is the velocity difference that develops across the grass tips and the outer flow, and δ is the thickness of this shear layer, in

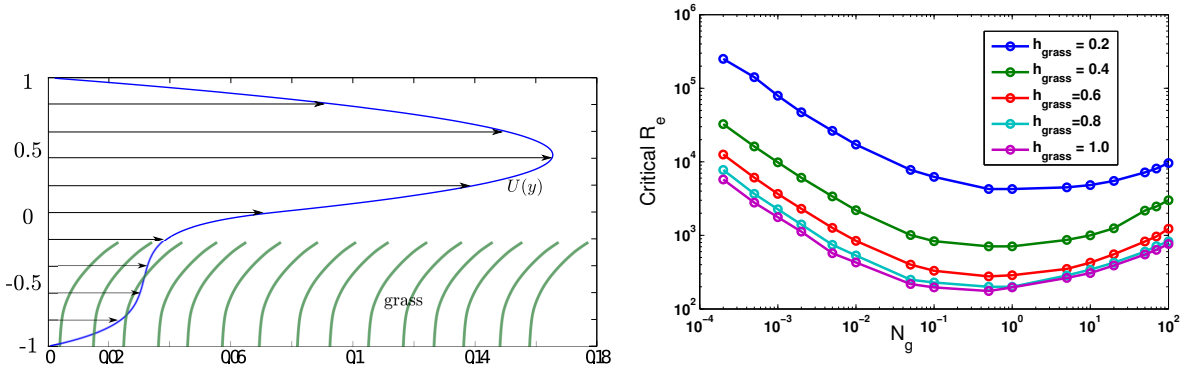

Figure 6: The steady background velocity profile from solving (15) (top) and the predicted critical Reynolds number for synchronous waving from solving (17) (bottom). This component of research is being performed in collaboration with *Amala Mahadevan, a physical oceanographer at WHOI and Lakshminarayanan Mahadevan, an applied mathematician at Harvard.*

agreement with the frequency of modes undergoing a Kelvin-Helmholtz shear instability[14]. The justification for the instability is stated as the inflection point in the uniform velocity field that develops as a result of the drag from the canopy, and Rayleigh's inflection point theorem. However, Rayleigh's theorem is valid for inviscid flow, and drag from the grass is not included in Rayleigh's analysis. Moreover, this mechanism does not obviously reveal a threshold in velocity for waving of the grass, as was observed in the field[15]. The threshold of waving is a critical condition to be aware of from the ecological perspective, because the transport properties are completely different in the presence and absence of waving. To help resolve these issues and to constructively contribute to an understanding of the induced mixing we perform a a linear stability analysis of the mathematical model.

The equations are non-dimensionalized using the flow velocity U_0, the water depth H and fluid density ρ, and the pressure is scaled such that its gradient is unity. For linear stability analysis, the flow velocity is decomposed into a steady uniform flow and a small perturbation as $\boldsymbol{u} = U(y)\boldsymbol{x} + \tilde{\boldsymbol{u}}$, where the steady state satisfies

$$\text{Inside grass: } \frac{d^2U}{dy^2} + 1 - \text{Re}N_g U^2 = 0 \qquad \text{Outside grass: } \frac{d^2U}{dy^2} + 1 = 0, \tag{15}$$

where, $\text{Re} = \rho U_0 H/\mu$ is the Reynolds number, N_g is the dimensionless grass density per unit area times the drag coefficient, and the 1 represent the background pressure gradient. This model for the steady flow has been carefully validated[34]. A sample equilibrium profile $U(y)$ is shown in figure 6.

The perturbation satisfies to linear order (dropping the tilde)

$$\text{Re}\,[u_t + Uu_x + U_y v + 2N_g Uu] = -p_x + \nabla^2 u, \quad \text{Re}\,[v_t + Uv_x] = -p_y + \nabla^2 v \tag{16}$$

Where N_g is zero outside grass. Eliminating pressure from above two equations, using stream function ψ, and substituting $(u, v, \psi) = (\hat{u}, \hat{v}, \phi)e^{ikx+\beta t}$, we get modified Orr-Sommerfeld

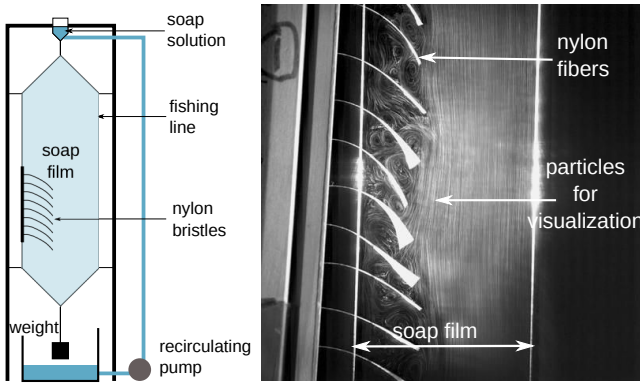

Figure 7: A schematic setup of the soap-film tunnel (left) and a sample over-exposed image to indicate the flow pattern past a periodic array of nylon filaments. Dripping soap solution expands into a soap film as it flows down under gravity to simulate the tidal flow, while the filaments mimic the grass blades. These experiments are being conducted in collaboration with *Mahesh Bandi, a physicist at Okinawa Institute of Technology, Japan.*

equation,

$$\mathrm{Re}(\beta + ikU)\left(D^2 - k^2\right)\phi = (D^2 - k^2)^2\phi + ikU_{yy}\phi - 2\mathrm{Re}N_g\left((U\phi_y)_y - U\phi_y\delta(y-h)\right), \quad (17)$$

where δ is the Dirac delta function. This equation poses an eigenvalue problem for the growth rate β, which we solve using finite difference. Critical Re obtained this way, as a function of non-dimensional grass density and grass height are shown in figure 6, and a sample eigenmode velocity field can be seen in figure 5. To ensure we are operating in the right parameter space, we compare the result with Grizzle, et al[15], who observed the grass to wave when the flow speed exceeded about 10 cm/s. The grass canopy they reported was about 2.5 m tall in a water of depth 3 m at threshold speed, and they did not report the grass blade area density, which we assume to be in the range 10^2 blades/m^2[33]. Using a representative $\mu = 0.5$ Pa-s as a typical value[33, 34], the Reynolds number for the observed threshold comes out to be about 600, which is within an order of magnitude of what is predicted by our analysis. Given the uncertainty in the actual grass density and the turbulent viscosity, this level of agreement is encouraging and prompts a detailed comparison.

We supplement this analysis with simple but informative experiments in our soap film tunnel, schematically shown in figure 7. An array of nylon filaments inserted in the flowing soap film start to oscillate synchronously if the flow is faster than a threshold. This system provides an excellent controlled environment to study the phenomena and compare with mathematical models (and hence the calculations with the no-slip boundary condition at the top boundary of the domain). Motion of microscopic glass particles inserted in the soap film and illuminated by a laser can be used to visualize the flow with a high-speed camera (Photron-SA5, see figure 7 for a sample snapshot), and perform particle image velocimetry (PIV) for quantitative information. Our first set of PIV images are being post-processed. So far, we have observed a close analogy between the two-dimensional experimental flow and

description of three-dimensional tidal flow, including the steady deformation, synchronized waving and even a threshold for its onset. The equipment budget requests funds for a laser system for illuminating the particles for visualization and PIV.

Knowing the flow field from the unstable eigenmode and the experimental visualization gives us a direct handle on all the transport behavior including the induced mixing. The weakly non-linear analysis is instrumental in confirming the preliminary experimental observation of hysteresis in the soap-film tunnel and also determining estimates of the amplitude of waving. Such information is crucial for constructing a complete picture of transport in vegetation canopies.

4 Trade-off as a constraint optimization problem

In this part, the mixing and waving of the grass is conceptually coupled with the optimal control of the hydrofoil motion. The coupling takes the form of constraints in the optimal control framework and boundary condition in the fluid-vegetation interaction. The downstream shed vorticity field is fed as an inlet boundary condition in the fluid-vegetation computation. The response of the vegetation and the transport is quantified, and must satisfy a suitable constraint in the form of one or more inequalities, depending on the idealized representation of our best understanding of the ecology. The identification of the constraints will be conducted in close collaboration with *Heather Leslie, an environmental ecologist at Brown.*

5 Naval relevance, impact and summary

The US potential for tidal in stream power derived from the kinetic energy of tidal currents is estimated at 50 GW[16] and tapping into this potential aligns with the Navy's goal to generate 50% of its shore-based electricity from alternative sources. Tidal current power densities are high (e.g. 500 W/m^2 in a flow of 1 m/s). Tides are predictable for centuries, and the resource is conveniently located near the shore for naval use. The converted energy is virtually free of carbon emissions. Moreover, small amounts of energy can be generated from ocean currents for deep sea operations and unmanned monitoring stations. The challenges underlying the successful adoption of tidal power include the development of technology suitable for this resource and the successful mitigation of the environmental impact.

We are planning and designing a pilot scale experiment for our commercialization project in calendar year 2013, with expected deployment in 2015, at which time we plan to extensively monitor the effect of tidal power conversion on marine habitats. The ONR YIP project in 2015 is expected to be at a stage analyzing the power ecology trade-off described in §4. The simultaneous conduction of both the theoretical analysis and field observations with systematic quantitative tools will benefit the long term goal maximally from the pilot scale experiments. The long term environmental impact of tidal power conversion are uncertain at worst and speculative at best[8], and this research not only provides a systematic method for analyzing the dependence, but also proposes a mechanism to mitigate the effects in the best possible way. Finally, the project is being developed by two graduate students advised by the PI, and the PI is committed to graduate education and training on topics of naval relevance. The majority of the budget requests funds to support the graduate students.

References

[1] J. Ackerman and A. Okubo. Reduced mixing in a marine macrophyte canopy. *Functional Ecology*, pages 305–309, 1993.

[2] S. Alben. Flexible sheets falling in an inviscid fluid. *Physics of Fluids*, 22:061901, 2010.

[3] N. Balmforth and S. Mandre. Dynamics of roll waves. *Journal of Fluid Mechanics*, 514(1):1–33, 2004.

[4] G. Batchelor. *An introduction to fluid dynamics*. Cambridge university press, 2000.

[5] R. Bedard, M. Previsic, O. Siddiqui, G. Hagerman, and M. Robinson. Survey and characterization: Tidal in stream energy conversion devices. Technical Report 1024638, EPRI, Palo Alto, 2011.

[6] P. Bell. Status of eutrophication in the Great Barrier Reef lagoon. *Marine Pollution Bulletin*, 23:89–93, 1991.

[7] P. Bell. Eutrophication and coral reefs—some examples in the Great Barrier Reef lagoon. *Water Research*, 26(5):553–568, 1992.

[8] G. Cada, J. Ahlgrimm, M. Bahleda, T. Bigford, S. Stavrakas, D. Hall, R. Moursund, and M. Sale. Potential impacts of hydrokinetic and wave energy conversion technologies on aquatic environments. *Fisheries*, 32(4):174–181, 2007.

[9] D. Cartwright. *Tides: a scientific history*. Cambridge University Press, 2000.

[10] A. Chorin. Vortex sheet approximation of boundary layers. *Journal of Computational Physics*, 27(3):428–442, 1978.

[11] J. Conover. The importance of natural diffusion gradients and transport of substances related to benthic marine plant metabolism. *Botanica marina*, 11(1-4):1–9, 1968.

[12] W. Dennison and D. Barnes. Effect of water motion on coral photosynthesis and calcification. *Journal of experimental marine biology and ecology*, 115(1):67–77, 1988.

[13] C. Garrett and W. Munk. Internal waves in the ocean. *Annual Review of Fluid Mechanics*, 11(1):339–369, 1979.

[14] M. Ghisalberti and H. Nepf. Mixing layers and coherent structures in vegetated aquatic flows. *Journal of Geophysical Research*, 107(C2):3011, 2002.

[15] R. Grizzle, F. Short, C. Newell, H. Hoven, and L. Kindblom. Hydrodynamically induced synchronous waving of seagrasses:'monami'and its possible effects on larval mussel settlement. *Journal of Experimental Marine Biology and Ecology*, 206(1):165–177, 1996.

[16] K. Haas. Assessment of Energy Production Potential from Tidal Streams in the United States. Technical report, Georgia Tech Research Corporation, 2011.

[17] P. Jokiel. Effects of water motion on reef corals. *Journal of Experimental Marine Biology and Ecology*, 35(1):87–97, 1978.

[18] M. Jones and M. Shelley. Falling cards. *Journal of Fluid Mechanics*, 540(1):393–425, 2005.

[19] E. Koch, J. Ackerman, J. Verduin, and M. Keulen. Fluid dynamics in seagrass ecology—from molecules to ecosystems. *Seagrasses: Biology, ecology and conservation*, pages 193–225, 2006.

[20] P. Kundu, I. Cohen, P. Ayyaswamy, and H. Hu. *Fluid Mechanics*. Academic Press. Academic Press, 2010.

[21] F. O. Lehmann. Wing–wake interaction reduces power consumption in insect tandem wings. *Animal Locomation*, page 203, 2010.

[22] J. Leichter, H. Stewart, and S. Miller. Episodic nutrient transport to Florida coral reefs. *Limnology and Oceanography*, 48(4):1394–1407, 2003.

[23] D. Lentink, W. B. Dickson, J. L. Van Leeuwen, and M. H. Dickinson. Leading-edge vortices elevate lift of autorotating plant seeds. *science*, 324(5933):1438–1440, 2009.

[24] M. Longuet-Higgins, E. Cokelet, M. Longuet-Higgins, and E. Cokelet. The deformation of steep surface waves on water. I. A numerical method of computation. *Proceedings of the Royal Society of London. A. Mathematical and Physical Sciences*, 350(1660):1–26, 1976.

[25] S. Mandre and M. P. Brenner. The mechanism of a splash on a dry solid surface. *Journal of Fluid Mechanics*, 690:148, 2012.

[26] S. Mandre and L. Mahadevan. A generalized theory of viscous and inviscid flutter. *Proceedings of the Royal Society A: Mathematical, Physical and Engineering Science*, 466(2113):141–156, 2010.

[27] S. Mandre, M. Mani, and M. P. Brenner. Precursors to splashing of liquid droplets on a solid surface. *Physical review letters*, 102(13):134502, 2009.

[28] M. Mani, S. Mandre, and M. P. Brenner. Events before droplet splashing on a solid surface. *Journal of Fluid Mechanics*, 647:163, 2010.

[29] L. McCook. Macroalgae, nutrients and phase shifts on coral reefs: scientific issues and management consequences for the Great Barrier Reef. *Coral reefs*, 18(4):357–367, 1999.

[30] S. Michelin and S. Llewellyn Smith. An unsteady point vortex method for coupled fluid–solid problems. *Theoretical and Computational Fluid Dynamics*, 23(2):127–153, 2009.

[31] S. Michelin and S. Llewellyn Smith. Falling cards and flapping flags: understanding fluid–solid interactions using an unsteady point vortex model. *Theoretical and Computational Fluid Dynamics*, 24(1):195–200, 2010.

[32] S. Michelin, S. Llewellyn Smith, and B. Glover. Vortex shedding model of a flapping flag. *Journal of Fluid Mechanics*, 617:1, 2008.

[33] H. Nepf. Drag, turbulence, and diffusion in flow through emergent vegetation. *Water resources research*, 35(2):479–489, 1999.

[34] H. Nepf and E. Vivoni. Flow structure in depth-limited, vegetated flow. *J. Geophys. Res*, 105(C12):28547–28557, 2000.

[35] S. Nixon. Physical energy inputs and the comparative ecology of lake and marine ecosystems. *Limnology and Oceanography*, pages 1005–1025, 1988.

[36] H. Parker. Influence of relative water motion on the growth, ammonium uptake and carbon and nitrogen composition of Ulva lactuca (Chlorophyta). *Marine Biology*, 63(3):309–318, 1981.

[37] C. Pozrikidis. *Boundary Integral and Singularity Methods for Linearized Viscous Flow*. Cambridge Texts in Applied Mathematics. Cambridge University Press, 1992.

[38] J. Sheng, A. Ysasi, D. Kolomenskiy, E. Kanso, M. Nitsche, and K. Schneider. Simulating Vortex Wakes of Flapping Plates. *Natural Locomotion in Fluids and on Surfaces*, pages 255–262, 2012.

[39] P. South and R. Mitchell. Oscillating wind energy conversion systems. *NASA STI/Recon Technical Report N*, 84:22018, 1983.

[40] R. B. Srygley and A. L. R. Thomas. Unconventional lift-generating mechanisms in free-flying butterflies. *Nature*, 420(6916):660–664, 2002.

[41] J. Stevenson. Comparative ecology of submersed grass beds in freshwater, estuarine, and marine environments. *Limnology and Oceanography*, pages 867–893, 1988.

[42] Z. J. Wang. Dissecting insect flight. *Annu. Rev. Fluid Mech.*, 37:183–210, 2005.

[43] D. R. Warrick, B. W. Tobalske, and D. R. Powers. Aerodynamics of the hovering hummingbird. *Nature*, 435(7045):1094–1097, 2005.

[44] W. Wheeler. Effect of boundary layer transport on the fixation of carbon by the giant kelp Macrocystis pyrifera. *Marine Biology*, 56(2):103–110, 1980.

[45] Q. Zhu. Optimal frequency for flow energy harvesting of a flapping foil. *Journal of Fluid Mechanics*, 675:495–517, 2011.

[46] Q. Zhu. Energy harvesting by a purely passive flapping foil from shear flows. *Journal of Fluids and Structures*, 2012.